Evolution of drop size distribution in natural rain

DOI: http://doi.org/10.1016/j.atmosres.2017.10.003

Evolution of Drop Size Distribution in natural rain

Leo Pio D'Adderio

Dep. of Physics and Earth Science, University of Ferrara, Italy,

Federico Porcù

Dep. of Physics and Astronomy, University of Bologna, Italy

Ali Tokay

JCET-University of Maryland Baltimore County and NASA-Goddard Space Flight Center, Greenbelt, Maryland, USA.

Corresponding author: Leo Pio D'Adderio, Department of Physics and earth Science, University of Ferrara, 44122, Ferrara, Italy
Email: dadderio@fe.infn.it

Abstract

Both numerical modeling and laboratory experiments document the possibility of a raindrop size distribution (DSD) to evolve to an equilibrium stage (EDSD), where all the principal processes occur at steady rates.

The aim of this work is to observe the temporal behavior of the DSD and to directly investigate the conditions favorable to the onset of the EDSD in natural rain. We exploited a large disdrometer dataset collected in the framework of the Ground Validation activities related to the NASA Global Precipitation Measurement mission. More than 200,000 one-minute data of two-dimensional video disdrometer (2DVD) are collected over USA to represent a wide range of precipitation types. The original data are averaged over 2 minutes and an automatic algorithm is used on a selected subset to identify samples with EDSD. Results show that the EDSD occurs mainly in convective events and lasts for very short time intervals (2 to 4 minutes). It is more frequent for rain rate between 20 and 40 mm h^{-1} and it mostly occurs during sharp increase of precipitation rates.

Keywords
Equilibrium Drop Size Distribution
Time evolution
Collisional breakup
Breakup detection algorithm
Radarmeteorology

1. Introduction

The Drop Size Distribution (DSD) is a fundamental property of precipitation and is widely investigated through laboratory, numerical modeling and field studies. A detailed knowledge of DSD structure and variability is required in remote sensor based precipitation retrieval algorithms (Tokay et al., 2016), in cloud resolving models (Tao et al. 2014) and in application to soil science and agriculture (Caracciolo et al, 2012).

From the cloud microphysics point of view, the DSD shape at the ground is determined in natural rain by the complex interplay of a number of mechanisms (Radhakrishna and Rao, 2009), where the collisional breakup is known as the process that limits the maximum raindrop size (McTaggart-Cowan and List, 1975; Barros et al., 2010). A large raindrop falling within or below a cloud and colliding with smaller drops, forms a larger raindrop when the Collisional Kinetic Energy (CKE) is lower than a limiting value (about 5 μJ), while larger CKE values indicate that the energy cannot be dissipated by the viscous motions of the merged drop, and the drop breaks up (Low and List, 1982a, Porcù et al., 2013). The drop disruption leads to a number of fragments with a well-defined distribution: one peak at size slightly smaller than the largest colliding drop, and one peak at very small drop size (Low and List, 1982a). Schlottke et al. (2010), who simulated the Low and List (1982a) experiment, found that collisional breakup takes place even for CKE slightly lower than 5 μJ, in cases of grazing collisions.

The combined effect of coalescence and collisional breakup has been studied mainly by simulations in numerical models, focusing on the shape variation of the initial DSD up to reach the so-called equilibrium stage, described by the Equilibrium DSD (EDSD). The parameterization proposed by Low and List (1982a,b) of breakup fragments is taken as reference in most of the numerical schemes to simulate DSD evolution in time until the EDSD is reached. While early studies concerning this topic found a three-peak EDSD (Valdez and Young, 1985; Brown, 1988; Feingold et al., 1988; Chen and Lamb, 1994), McFarquhar (2004) derived a different parameterization of the breakup fragments, leading to a different shape of the EDSD with respect to the previous works. Starting from an initial exponential DSD corresponding to 54 mm h^{-1} rainfall rate, the resulting EDSD presents a bi-modal shape with the peaks at 0.26 and 2.3 mm. Prat and Barros (2007), using a discrete model, found that the EDSD has the same shape (bi-modal) independently from the initial DSD and for the same rainfall rate and breakup kernel, with marked difference in the time required to reach the EDSD. In their follow-up studies, deepening the influence of the microphysical processes on Z-R relationship (Prat and Barros, 2009), they found that, in general, for rain rates lower than 20 mmh^{-1} the coalescence is the dominant process. For higher rain rates, the breakup is the dominant process and the time to reach the EDSD is about half as long as in the case of light rainfall (about 30 minutes compared with at least one hour). Moreover, they found that for heavy rain the sensitivity of the DSD shape to the rain rate is negligible. More recently, Prat and Barros, (2012) developed a new parameterization of the fragments of the drop-drop collision leading to EDSD with a lower number of large drops. This evidences that the EDSD can be reached at lower rainfall rate regimes than what they previously found.

As also highlighted by McFarquhar (2004), the literature is scant of EDSD observations from natural rain. While the numerical model outputs allow for monitoring rain DSDs resulting from coalescence and breakup events at every time stamp, thus unambiguously assessing the EDSD onset, the detection of EDSD in natural rain is more questionable. Hu and Srivastava (1995) tried to compare their model output with disdrometer observations noticing that in addition to the bi-modal shape, a slope in the large drops tail of observed DSD around 20 cm^{-1} can be taken as a signature of EDSD, shaped by collisional processes. However, this result could be affected by the known problem of Joss Waldvogel disdrometer in detecting large drops.

A further characteristic of the EDSD is the bi-modality. Porcù et al. (2013, 2014) observed bi-modal DSD shape from measurements at different altitudes using a low power X-band Doppler disdrometer. The position of the DSD peaks agrees quite well with that obtained by different numerical models, even though there was altitude dependence. Bi-modal DSDs were also observed by Steiner and Waldvogel (1987), Zawadzki and de Agostinho Antonio (1988), List et al. (1988), and Asselin de Beauville et al. (1988), which all used Joss-Waldvogel disdrometer. Willis and Tattelman (1989) also observed bi-modal DSD at very high rainfall rates collected during hurricanes and tropical storms using an optical spectrometer. However, bi-modality does not seem to be a sufficient condition to have EDSD, since other cloud processes are able to produce bi-modal DSD (Radhakrishna and Rao, 2009). Based on both theoretical studies and experimental observations, D’Adderio et al. (2015) developed an automatic algorithm to identify bi-modal DSD (with peaks in well defined diameter ranges) and labeled them as EDSD, analyzing two-minutes samples from six different field campaigns. They found that, in natural rain, the reaching of the EDSD is rare (at most 7% of the analyzed samples) and occurs mainly during convective precipitation.

In this paper, by using the D’Adderio et al. (2015) algorithm, the conditions favorable to reach the EDSD in natural rain have been studied. To this end, an extensive disdrometer dataset, collected during several field campaigns in the framework of the NASA/JAXA Global Precipitation Measurement Mission (GPM) ground validation (GV) activities, is analyzed to extract EDSD samples in natural rain. The automatic algorithm developed by D’Adderio et al. (2015), based on the slope of the DSD curve between 1.0 and 2.6 mm, is used to select the EDSD samples as collected by the two-Dimensional Video Disdrometer (2-DVD).

We remark that the GPM GV field campaigns, although providing a large amount of high quality disdrometric data, were not planned to study DSD properties at cloud scale. A dedicated field campaign would be desirable to complete the results of the present work allowing a lagrangian observation of the cloud to assess the full temporal evolution of the EDSD in the same developing cloud column.

The paper is organized as follow: Section 2 presents a brief description of the field campaigns characteristics useful to our aim; a critical description of the algorithm to identify the EDSD is given in Section 3, while Section 4 and Section 5 describe the overall results obtained and some case study, respectively. The last section provides the conclusions.

2. Field Campaigns characteristics

This study uses the 2DVD (Schönhuber et al. 2007) observations from five different field campaigns of the GPM-GV program: Iowa Flood Studies (IFloodS – 41.6N, 91.5W from May 1 to June 15, 2013), Midlatitude Continental Convective Clouds Experiment (MC3E – 36.7N, 97.1W from April 22 to June 6, 2011), Wallops Flight Facility (Wallops – 37.5N, 75.5W from July 22, 2013 to October 7, 2015 not continuously), Integrated Precipitation and Hydrology Experiment (IPHEx – 35.5N, 82.5W from May 1 to June 15, 2014) and Alabama-Huntsville (Alabama – 35N, 87W from December 17, 2009 to October 13, 2011). The drop-by-drop raw output of the 2DVD was binned in 0.2 mm bin width and averaged over two minutes, called samples hereafter. Table 1 summarizes the characteristics of 2DVD observations relevant for our analysis in each field campaigns. The rightmost column reports the samples with positive Highest Slope (HS), which is the maximum slope of the linear fit of the DSD between 1.0 and 2.6 mm, defined in D’Adderio et al. (2015) that will be discussed in the next Section.

Field Campaign	Events	Samples	Stratiform Samples	Convective Samples	HS>0 Samples
Alabama	4	68		68	7
IFloodS	28	1016	63	953	48
IPHEx	14	368		368	28
MC3E	10	174		174	13
Wallops	75	1466	31	1435	133

Table 1. Characteristics of the dataset.

The number of rainfall events considered in the present work ranges from 4 for the Alabama dataset to 75 for the Wallops site (Table 1). An event is defined as set of at least 8 samples with rain rate exceeding 1 mm h^{-1} and reporting at least one EDSD selected according to the D'Adderio et al. (2015) algorithm. This has been considered a good compromise between having a sufficient time interval to follow the evolution of the precipitation, and to include stratiform precipitation that could lead to EDSD. Each event is identified as convective or stratiform according to Bringi et al. (2003): the classification is based on the standard deviation of the rain rates. If the standard deviation of the rain rates is ≥ 1.5 mmh^{-1}, then the event is considered convective otherwise it is considered stratiform. Ioannidou et al. (2016) used the same criterion to validate the measurements of the Precipitation Radar (PR) of the Tropical Rainfall Measuring Mission (TRMM) by comparing the rainfall estimates with 2DVD and X-band ground based radar measurements. Several authors conducted studies about the development of technique to characterize convective and stratiform precipitation. Among the others, Caracciolo et al. (2006) based their analysis using high order DSD moments, while Thurai et al. (2016) developed a separation technique in the N_w-D_0 space. Table 1 also shows that almost all the selected samples are classified as convective, while the last column reports the number of samples with EDSD occurrence.

Table 2 reports, for each dataset, the number of all registered convective and stratiform episodes, considered just as set of at least 8 samples with rain rate exceeding 1 mm h^{-1} regardless if EDSD is present or not. The percentage of episodes with EDSD (previously defined as event) ranges between

17 and 27% of cases selected according to our classification. All the datasets report a significant number of stratiform episodes, even if only three present at least one EDSD sample. This aspect highlights the strict relationship between the onset of EDSD and the convective precipitation.

Field Campaign	All Convective	Convective with EDSD	All Stratiform	Stratiform with EDSD
Alabama	15	4	12	0
IFloodS	143	26	123	2
IPHEx	80	14	33	0
MC3E	54	10	54	0
Wallops	154	74	212	1

Table 2. Convective/stratiform classification for the registered episodes.

Figure 1 shows the Probability Density Function (PDF – blue lines) and Cumulative Density Function (CDF – red lines) of rain rate for the considered events (3,092 samples) after the convective/stratiform discrimination (solid/dashed lines).

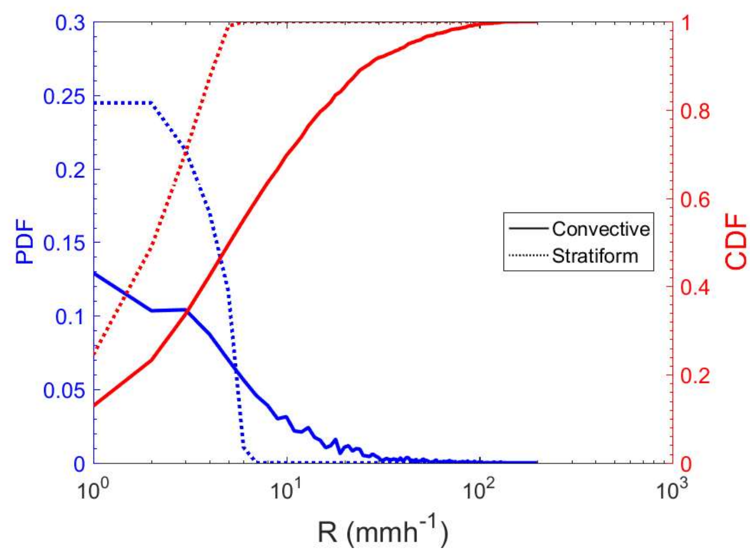

Figure 1. PDF (blue lines) and CDF (red lines) for convective (solid lines) and stratiform (dashed lines) samples.

The rain rate of the stratified events presents a narrow distribution and never exceeds 7 mm h^{-1} with a marked peak around 2 mm h^{-1}. The PDF of the convective events is toward higher values, up to more than 100 mmh^{-1}, and about the 30% of the samples has rain rate exceeding 10 mm h^{-1}.

3. Equilibrium Drop Size Distribution detection algorithm

Following laboratory experiment results (Low and List, 1982a, b) and numerical modeling output (Prat and Barros, 2012), the EDSD bi-modal shape is characterized by: 1) a peak at very small drops end (around 0.3 mm) due to the breakup fragments; 2) a depletion in the region between 1.0 and 1.5 mm due to the drops involved in the collisions; 3) a relative secondary maximum around 2.0 mm. This is well observed in numerical simulations, where the EDSD shape is reached after a given time following the start of precipitation, and lasts indefinitely until a modification in the boundary conditions occurs (Prat and Barros, 2009).

An automated algorithm based on the slope (HS) of the linear fit of the DSD between 1.0 and 2.6 mm has been introduced to identify and select the EDSD in natural rain (D'Adderio et al, 2015). The EDSD is present if the sample satisfies the condition HS>0, i.e. the DSD shape shows the same features found in EDSD obtained by numerical modeling and laboratory experiments. This algorithm is applied to the samples with rain rate exceeding 5 mmh^{-1}, and the events where at least one sample has HS>0 have been selected for further processing.

As a matter of fact, the algorithm selects the DSD with positive slope between 1 and 2.6 mm in the diameter spectrum, which have been labeled as EDSD (D'Adderio et al, 2015). We are aware that other mechanisms can induce bi-modality in DSD: size sorting (related to updraft and vertical wind shear or to the beginning of the precipitation), coexistence of melted snowflakes and supercooled droplets, rainshafts overlapping, and any combination of these (Radhakrishna and Rao, 2009). It is difficult, if not impossible, to assess the contribution of each mechanism by analyzing the DSD shape in natural rain. We based the reliability of the results of the algorithm in identifying the EDSD on the correspondence with numerical studies and the discussion below.

In order to quantify the possible influence of the above-mentioned mechanisms in the EDSD selection, the detection algorithm has been applied to a wider diameter spectrum, between 0.6 and 5.0 mm, seeking for HS>0. We found 352 DSD samples, distributed with the size of the point corresponding to HS>0 as shown in Figure 2. For most of the selected DSD (180; 51%) this point is in the interval 1.0-2.6 mm, a large fraction (127; 36%) is between 0.6-1.0 and the reminders (45; 13%) are distributed above 2.6 mm. Most of the DSD with positive HS in the interval 0.6-1.0 mm are not bi-modal but can be due to the underestimation of small drops by 2DVD (Tokay et al. 2013) resulting in a peak between 0.5 and 1.0 mm. The rest of the graph shows that positive HS can be found along the diameter spectrum for all values, but its occurrence is much more frequent in the 1.0-2.6 interval. This analysis, in our view, supports our hypothesis of labeling as EDSD the DSD with positive HS in this interval, since the other mentioned mechanisms producing bi-modal DSD are expected to be distributed randomly without any preferential size. Even if we are confident that the DSD with positive HS in the interval 1.0-2.6 mm are EDSD, we cannot exclude a marginal contamination from DSD for which bi-modality is not due to equilibrium.

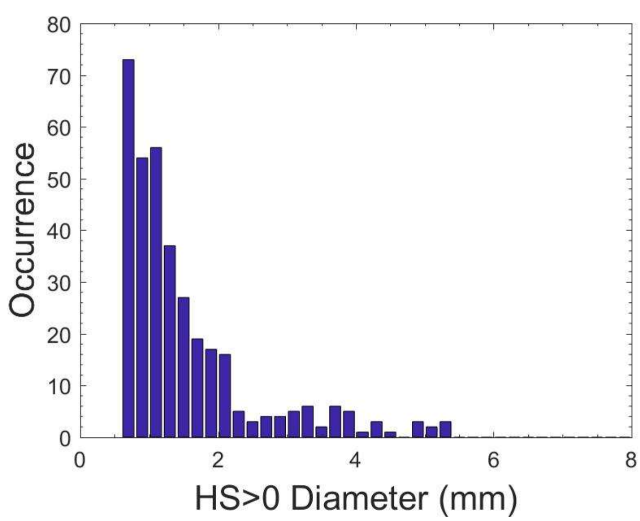

Figure 2. Distribution of drop diameter corresponding to HS>0 when the identification algorithm (D’Adderio et al., 2015) is applied to 0.6-5 mm range.

Several arguments makes the effects of sorting unlikely in shaping the DSD: 1) the 2DVD sampling volume is rather small (around 11 m^3 for largest drops), and thus making influences of size sorting in rain volumes unlikely, as it is more common in radar data (Dawson et al., 2015); 2) generally size sorting DSD presents a marked peak for large drops (2 mm of diameter or more), and with few drops at small size (Kumjian and Ryzhkov, 2012). Among the 352 DSD only 18 show a signal that can be due to size sorting contamination, with the peak at larger size (above 1.3 mm) higher than the peak at smaller drop size, while we never observed DSD with single peak at diameters larger than 2 mm. Finally, the possible contamination from DSD shaped by the coexistence of melted ice flakes and supercooled drops (or other anomalous distribution of frozen hydrometeors aloft) is unlikely, given the fact that the freezing level during the considered events is always higher than 2500 m a.s.l..

4. Results

A first analysis was devoted to assess the occurrence of EDSD in convective and stratiform events: Figure 3 shows each sample according to its rain rate and HS value. EDSD occurrence in stratiform events is very rare and only three events in IFloodS and Wallops datasets (see Table 2) reported only three samples with EDSD (i.e. HS>0). The rain rate of the EDSD (i.e. HS>0) ranges mainly between 5 and 70 mm h^{-1}, while at higher rain rates, even exceeding 100 mm h^{-1}, the HS values is centered around -0.5 $mm^{-3}m^{-2}$. In general, higher rain rates have lower HS values even if positive, while lower rain rates can reach HS values larger than one, indicating a marked two-peak DSD.

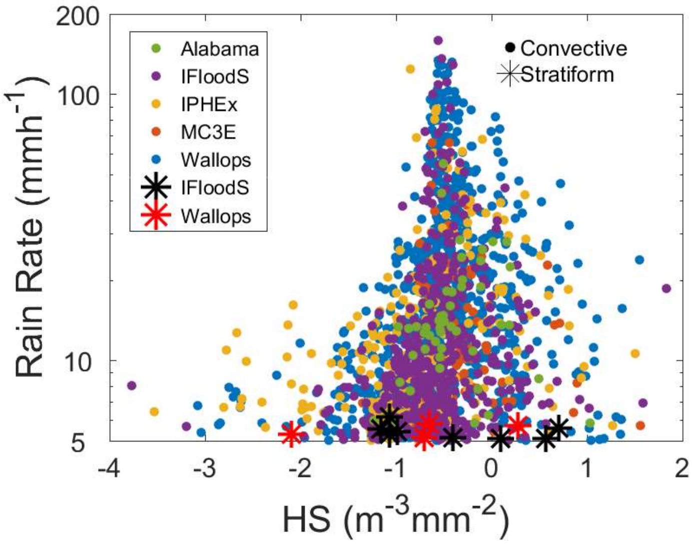

Figure 3. Distribution of the samples belonging to the selected events according to their rain rate and HS. Dots indicate convective samples, while stars indicate stratiform samples.

The dependence of EDSD occurrence on the rain rate is presented by considering the fraction of EDSD samples as function of the rain rate sampled over 6 mm h^{-1} wide intervals (Figure 4). The fractional occurrence of EDSD slightly increases with the rainfall rate to reach a maximum above 17% around 40 mm h^{-1}, while the probability to have EDSD decreases below 10% at higher rain rates.

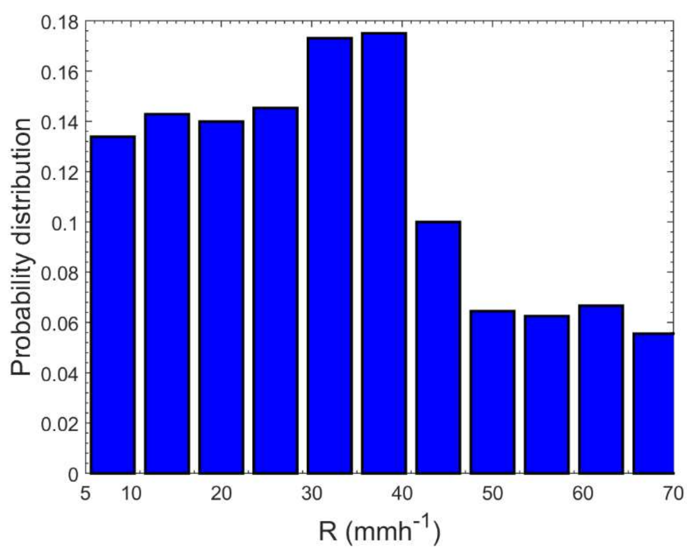

Figure 4. Fractional occurrence of samples with EDSD (HS>0) as function of the corresponding rain rate.

The onset of EDSD seems to be weakly related to rainfall intensity above the threshold used. To assess if the EDSD is sensitive to the change of the rainfall intensity, the percent rain rate difference between two consecutive samples is calculated and, for each value, the percentage of samples with EDSD is reported at 20% intervals (Figure 5). Results indicate that a sudden increase of precipitation rate (especially between 100 and 200%) is favorable to the occurrence of EDSD. The samples where the rainfall rate increases between 120 and 200% have the probability higher than 30% to have EDSD, with a peak of 45% for a relative increase of rain rate of 150%. A sudden decrease of rainfall rate between two consecutive samples, shows a very low occurrence (about 2%) of EDSD, as well very large positive rain rate variation (above 220%) does not present any EDSD.

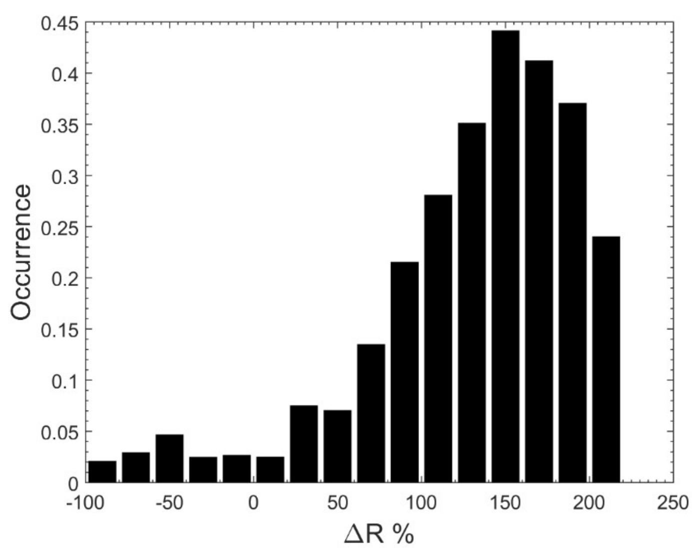

Figure 5. Fractional occurrence of samples with HS>0, as function of the relative rain rate difference between each sample and the previous one.

A further analysis has been devoted to understand how the DSD evolves in time to reach the equilibrium stage. The delay (in minutes) between the first rain detection for each event and the appearance of the EDSD is computed for all the dataset (Figure 6). Each bar is two-minutes width and it is centered in the middle value of the class (i.e. the first bar is centered at minute one and indicated the detection of EDSD at first or second minute of the considered event).

The distribution is clearly peaked for time delays between 2 and 8 minutes after the precipitation is first detected: for the 80% of the EDSD observation, it takes place within 20 minutes from the start of the event observation, and in the 10% of the cases, the EDSD coincides with the first observation of the event. There are also very few events for which the EDSD takes place after a long time (between 60 and 90 minutes). EDSD was observed only once in an event in most of the observations (75%), while two consecutive EDSD samples were present only in the 6% of the time. Longer period with EDSD continuously detected are even rarer: 10 and 2 times (around 4 and 1% of the EDSD samples) for 3 and 4 consecutive EDSD, respectively. Moreover, in the 15% of the cases EDSD appears two or more times (not consecutively) in different stages of the same event.

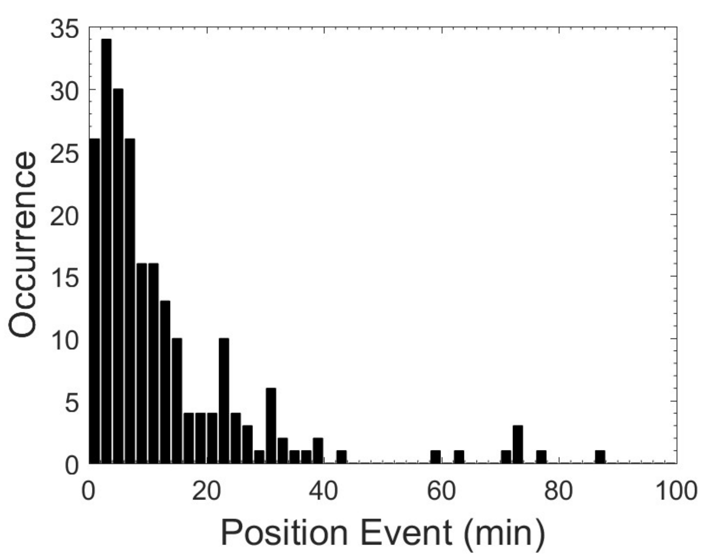

Figure 6. Number of samples with HS>0 as function of the time difference with respect to the first observation of the event (i.e. RR>1 mm h^{-1}).

With our observing system (fixed and point-like measurements), however, we are not able to follow separately the spatial and time evolution of the same cloud column, and thus we cannot unambiguously assess the time needed to a given cloud column to reach the EDSD. This limitation prevents a deeper analysis of the results, and we discussed EDSD properties not affected by the inadequacy of the experimental settings. A field measurement designed for this purpose, however, would require a very high density disdrometers network with a focused spatial distribution and a dedicated radar with a high temporal resolution (given the fast response of the transient EDSD) to follow the evolution of the precipitation pattern.

5. Case studies

Times series of rain rate and HS are presented for three cases: two illustrate how the EDSD is reached in convective cases, and one will describe a stratiform case where the EDSD is not reached despite its long duration.

5.1 Convective events

The convective events selected show at least one EDSD spectrum during their lifetime. The time evolution of HS can be explained according to the time of observation of the EDSD occurrence with respect to the rain rate peak and the start of the observation. The analysis leads to the division of the selected events in two main groups.

For the events belonging to the first group, rainrate is already high at the first observation, and the HS is positive in one of the first samples: in more than 10% of the cases (Figure 6), the first sample observed in an event has a relatively large positive HS value, indicating that the EDSD is found in proximity of the edge of the rain pattern at the beginning of the rain event observation. We interpret this behavior as follows: the rain system overpasses the instrument when the rain column already reached a mature stage. Often rain rate keeps increasing with time while HS drops below zero, indicating that the EDSD is lost due to the passage of the most intense part of the weather system over the instrument.

The second group of events is characterized by light/moderate rain rate and negative HS value at the beginning of the observation, rain rate increases more slowly with time, and reaches maximum values within 15-25 minutes after the first observation. HS increases in parallel with rain rate, reaching a positive value in correspondence with the maximum rain rate. We observe, in this case, the transition between negative and positive HS values, related to the increase of rain rate.

We present two case studies to illustrate the first and second group.

The event occurred on October 20, 2013 during the IFloodS field campaign is an example of well-defined convective event, belonging to the first group, where rain rates reached 160 mmh^{-1} (Figure 7a). Measured rain rate increased from 4 to 44 mm h^{-1} in two minutes, and the first positive HS value was found by the algorithm at minute 204. The HS then dropped down below zero indicating that the EDSD signal was lost while rain rate further increased, and HS oscillates around -0.5 $m^{-3}mm^{-2}$ after the peak rain rate (R = 159 mm h^{-1}) at minute 210. A close inspection of the DSD of minute 204 and minute 210 (Figure 7b), shows an EDSD with a marked depletion of drops around 2 mm, that evolves to a DSD with much more drops until 4.5 mm and a well-defined slope. However, a weak change of concavity is present between 1 and 3 mm, indicating that other processes (Radhakrishna and Rao 2009), occurring during such intense episodes, affect the equilibrium between breakup and coalescence, and prevent the maintenance of the EDSD.

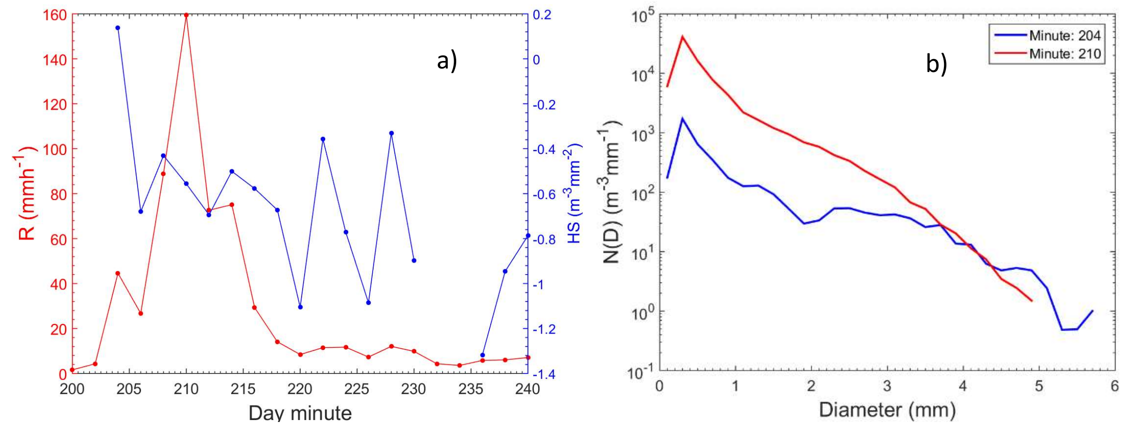

Figure 7. a) Time series of rain rate (red dot-line) and HS (blue dot-line) values, and b) DSDs of two samples of a rain event occurred on May 20, 2013 during IFloodS field campaign.

A second convective case, occurred on May 15, 2014 during the IPHEX field campaign, is reported to represent the second groups of events. In this case, HS reached its positive value at the peak of rain rate. The HS constantly increases from the beginning of the observation (except for one sample where a marked decrease of HS is related to a marked decrease of rain rate), up to reach a positive value. The precipitation peak reaches lower value with respect to the previous case, and this is a general difference between the two groups: the average peak intensity is 60.6 mmh^{-1} and 36.3 mm h^{-1} for the first and the second group, respectively. On the other hand, the mean rain rate of the EDSD samples does not show any difference for the two groups, with 14.8 and 13.8 mmh^{-1} for the first and second group, respectively. The higher rain rates do not seem support the developing and maintaining of EDSD. Furthermore, this case also confirms the transient nature of the EDSD, with its extremely short duration (only one sample).

The analysis of the DSD (Figure 8b) shows a clear transition from a well-defined Gamma distribution shape at minute 380 (green line) and at minute 382 (red line), both with μ parameter around 4.8, to a bi-modal shape indicating the EDSD occurrence. Minute 384 (blue line) evidences the breakup effects with a concavity change already present leading to EDSD at minute 386 (black line).

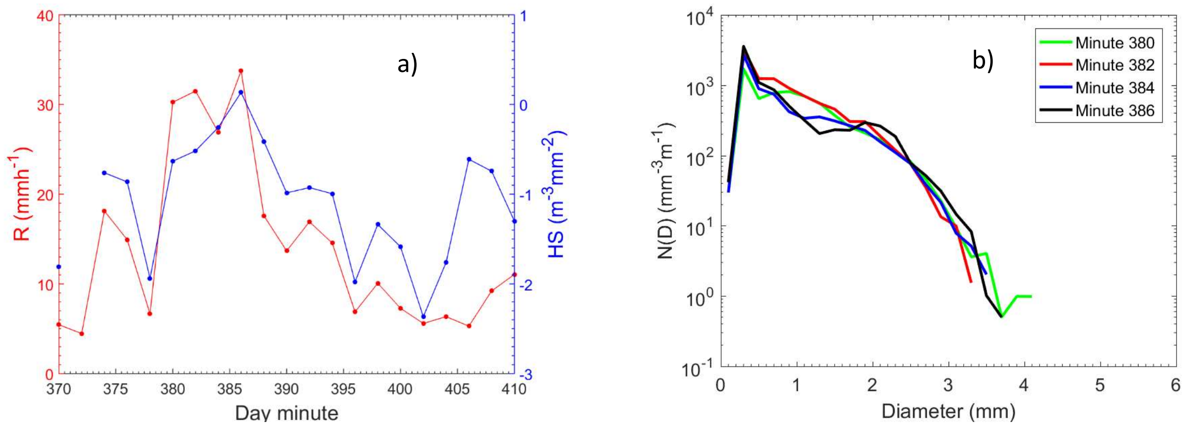

Figure 8. a) The same of Figure 6a, but for the event occurred on May 15, 2014 during IPHEX field campaign; b) DSDs preceding the equilibrium stage and EDSD.

5.2 Stratiform episode

The time evolution of rain rate and HS is shown for a stratiform case, occurred on December 29, 2013 at Wallops Island, Virginia, not classified as event since HS never reaches positive values (Figure 9). This case was observed for more than one hour and the rain rate was between 5 and 10 mm h^{-1}. The HS parameter at the beginning of the observation had high negative value, indicating a very steep DSD, with a relatively large amount of small drops and no drops with diameter larger than 2 mm. The HS increases rapidly, indicating the formation of larger drops, as effect of coalescence, and then keeps increasing slowly with time, reaching the highest value after 60 minutes of nearly constant rain intensity, still lower than zero (Figure 9a). This shows that along the event the DSD modifies, reducing the slope of the curve between 1.0 and 2.6 mm. Comparing our results with Prat and Barros (2009) numerical simulations, this case demonstrates that time necessary to reach the EDSD during a stratiform event could be much longer with respect to a convective event.

The DSD of the considered event does not present any particular characteristic (Figure 9b). The measured drop diameters are generally lower than 3.5 mm, well below the breakup size (Porcù et al, 2013), therefore no bi-modal shape can be identified within this event.

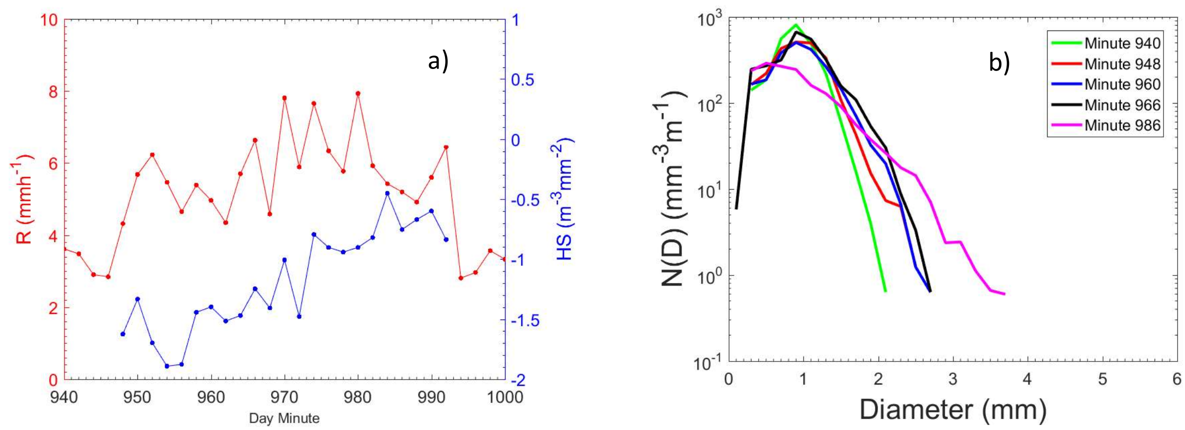

Figure 9. a) The same of Figure 6a, but for December 29, 2013 at Wallops Island, Virginia; b) sampling of DSDs for the whole period of observation.

Conclusions

High density, high quality disdrometric datasets have been analyzed to investigate the DSD dynamics in natural rain. A specific algorithm developed to identify bi-modal DSD is applied to more than 6,000 minutes of liquid precipitation 2DVD measurements collected in different seasons and locations. We propose a number of arguments to assess that these bi-modal DSD are EDSD, allowing the analysis of their temporal characteristics.

Our results demonstrate that EDSD is reached almost exclusively in convective rain (128 convective events and 3 stratiform events), and confirm that the onset of EDSD is a rare event in natural rain (Prat and Barros, 2012) occurring at most around 7% of the times (D’Adderio et al., 2015).

We found that EDSD shows up few minutes after the start of the observation (about 66% in the first 10 minutes), indicating that EDSD is more likely to take place in the proximity of the external edge of the rain area. Since most of the considered events have a total duration of around 20-30 minutes, thus, we can extrapolate that the onset of the EDSD is expected to take place 10-15 minutes after the beginning of the precipitation, confirming the time scales suggested by numerical modeling.

A second relevant feature is the short lifetime of the EDSD, observed in only one 2-minute sample in most of the cases (about 75% of the cases). EDSD, moreover, is often detected in cases of relatively rapid precipitation rate increase. The probability to have an EDSD exceeds 25% for those samples presenting a rain rate increase of more than 100% with respect to the previous sample, with a relative maximum higher than 45% of EDSD occurrence when the fractional increase of rain rate is around 150%. In the case of the maximum rain rate observed is very high (above 50 mm h^{-1}) the EDSD signal is lost, due to a number of mechanisms of higher order of complexity with respect to the coalescence-breakup balance (Radhakrishna and Rao 2009). If the rainfall rate remains limited below 50 mm h^{-1}, is more frequent to find the EDSD in correspondence to the maximum rain rate.

For a group of events the instrument does not observe the precipitation onset: at a certain stage of the precipitation column life, the system reaches the instrument (we deducted this since the first sample presented high rain rate values) and the measurement starts from the external part of the rain column, where EDSD is detected. For a second group of events, the instrument observes the early stages of precipitation development until a maximum rain rate is reached: HS growths with rain intensity (starting from very low values) and maximum rainrate and EDSD are observed at the same time. In case of stratiform episodes, the DSD changes in time, increasing the drop size, but reaches equilibrium in only three cases.

The observation of the time evolution of DSD in natural rain is a difficult task, since it would need Lagrangian measurements of the cloud column. With our Elulerian approach, however, we assess some basic properties of the onset of the EDSD, compatible with numerical modeling and laboratory results. The results and related comments we reported in this work would be confirmed by an ad hoc experimental campaign, which seems, however, difficult to design and carry on.

Acknowledgements

This study was partially funded by the “The Foundation BLANCEFLOR Boncompagni Ludovisi, née Bildt”. Thanks to Patrick N. Gatlin of NASA Marshall Space Flight Center and Matthew Wingo of the University of Alabama at Huntsville for maintenance of 2DVD during NASA Global Precipitation Measurement (GPM) mission ground validation field campaigns led by Walter Petersen of NASA Wallops Flight Facility.

References

Barros, A. P., Pratt O. P., and Testik F. Y., 2010: Size distribution of raindrops. Nat. Phys., 6, 232.

Bringi V.N., Chandrasekar V., Hubbert J., Gorgucci E., Randeu W. L., and Schoenhuber M., 2003: Raindrop Size Distribution in Different Climatic Regimes from Disdrometer and Dual-Polarized Radar Analysis. J. Atmos. Sci., 60, 354–365.

Brown, P. S., Jr., 1988: The effects of filament, sheet, and disk breakup upon the drop spectrum. J. Atmos. Sci., 45, 712–718, doi: 10.1175/1520-0469(1988)045<0712:TEOFSA>2.0.CO;2.

Caracciolo, C., Prodi, F., Battaglia, A., Porcù, F., 2006. Analysis of the moments and parameters of a gamma DSD to infer precipitation properties: a convective stratiform discrimination algorithm. Atmos. Res. 80 (2–3), 165–186.

Caracciolo, C., Napoli M., Porcù F., Prodi F., Dietrich S., Zanchi C. and Orlandini S., 2012: Raindrop size distribution and soil erosion. J. Irrig. Drain Eng., 138, 461-469.

Chen, J.-P. and Lamb D., 1994: Simulation of Cloud Microphysical and Chemical Processes Using a Multicomponent Framework. Part I: Description of the Microphysical Model. J. Atmos. Sci., 51, 2613-2630, DOI: http://dx.doi.org/10.1175/1520-0469(1994)051<2613:SOCMAC>2.0.CO;2.

D'Adderio L.P., Porcù F. and Tokay A., 2015: Identification and analysis of collisional break-up in natural rain. J. Atmos. Sci., 72, 3404-3416, DOI: 10.1175/JAS-D-14-0304.1.

Dawson, D.T. II, Mansell, E.R. and Kumjian, M.R., 2015: Does wind shear cause hydrometeor size sorting, J. Atmos. Sci., 72, 340-348

Feingold G., Tzivion (Tzitzvashvili) S. and Leviv Z., 1988: Evolution of Raindrop Spectra. Part I: Solution to the Stochastic Collection/Breakup Equation Using the Method of Moments. J. Atmos. Sci., 45, 3387-3399, DOI: http://dx.doi.org/10.1175/1520-0469(1988)045<3387:EORSPI>2.0.CO;2

Ioannidou M.P., Kalogiros J.A., Stavrakis A.K., 2016: Comparison of the TRMM Precipitation Radar rainfall estimation with ground-based disdrometer and radar measurements in South Greece. Atmos. Res., 181, 172-185, DOI: http://dx.doi.org/10.1016/j.atmosres.2016.06.023

Kumjian M.R. and Ryzhkov A.V., 2012: The Impact of Size Sorting on the Polarimetric Radar Variables. J. Atmos. Sci., 69, 2042-2060. DOI: 10.1175/JAS-D-11-0125.1

Low, T. B., and List R., 1982a: Collision, coalescence and breakup of raindrops. Part I: Experimentally established coalescence efficiencies and fragment size distributions in breakup. J. Atmos. Sci., 39, 1591–1606, doi:10.1175/1520-0469(1982)039,1591:CCABOR.2.0.CO;2.

Low, T. B., and List R., 1982b: Collision, coalescence and breakup of raindrops. Part II: Parameterizations of fragment size distributions. J. Atmos. Sci., 39, 1607–1618, doi:10.1175/ 1520-0469(1982)039,1607:CCABOR.2.0.CO;2.

McFarquhar G. M., 2004: A new representation of collision-induced breakup of raindrops and its implications for the shapes of raindrop size distributions. J. Atmos. Sci., 61, 777–794.

McTaggart-Cowan, J.D. and List R., 1975: Collision and breakup of water drops at terminal velocity. J. Atmos. Sci., 32, 1401–1411.

Porcù, F., D'Adderio L. P., Prodi F. and Caracciolo C., 2013, Effects of altitude on maximum raindrop size and fall velocity as limited by collisional breakup, J. Atmos. Sci., 70, 1129-1134.

Porcù, F., D'Adderio L. P., Prodi F. and Caracciolo C., 2014, Rain drop size distribution over the Tibetan Plateau, Atmos. Res., 150, 21-30.

Prat, O. P. and Barros A. P., 2007: A Robust Numerical Solution of the Stochastic Collection–Breakup Equation for Warm Rain. J. App. Meteor. Climatol. 46, 1480-1497.

Prat, O. P. and Barros A. P., 2009: Exploring the transient behavior of Z-R relationships-Implications for Radar Rainfall Estimation. J. Applied Meteor. and Clim., 48, 2127-2143.

Prat, O. P., Barros A. P. and Testik F., 2012: On the influence of raindrop collision outcomes on equilibrium size distributions. J. Atmos. Sci., 69, 1534–1546, doi:10.1175/JAS-D-11-0192.1.

Radhakrishna, B., and Rao T. N., 2009: Statistical characteristics of multipeak raindrop size distributions at the surface and aloft in different rain regimes. Mon. Wea. Rev., 137, 3501–3518, doi:10.1175/2009MWR2967.1.

Schlottke, J., Straub W., Beheng K., Gomaa H., and Weigand B., 2010: Numerical investigation of collision-induced breakup of raindrops. Part I: Methodology and dependencies on collision energy and eccentricity. J. Atmos. Sci., 67, 557–575, doi:10.1175/2009JAS3174.1.

Schönhuber, M., Lammer G., and Randeu W. L., 2007: One decade of imaging precipitation measurement by 2Dvideo-disdrometer. Adv. Geosci., 10, 85–90, doi:10.5194/adgeo-10-85-2007.

Steiner, M. and Waldvogel A., 1987: Peaks in Raindrop Size Distributions. J. Atmos. Sci., 44, 3127-3133, DOI: http://dx.doi.org/10.1175/1520-0469(1987)044<3127:PIRSD>2.0.CO;2.

Tao, W.-K., Lang S., Zeng X., Li X., Matsui T., Mohr K., Posselt D., Chern J., Peters-Lidard C., Norris P.M., Kang I.-S., Choi E., Hou A., Lau K.-M. and Yang Y.-M., 2014: The Goddard Cumulus Ensemble model (GCE): Improvements and applications for studying precipitation processes. Atmos. Res., 143, 392–424

Thurai M., Gatlin P.N., Bringi V.N., 2016. Separating stratiform and convective rain types based on the drop size distribution characteristics using 2D video disdrometer data. Atmos.Res., 169, 416-423. DOI: ttp://dx.doi.org/10.1016/j.atmosres.2015.04.011

Tokay, A., W. A. Petersen, P. Gatlin, and M. Wing, 2013: Comparison of raindrop size distribution measurements by collocated disdrometers. J. Atmos. Oceanic Technol., 30, 1672-1690.

Tokay, A., D'Adderio L.P., Wolff D. B. and Petersen W. A., 2016: A Field Study of Pixel-Scale Variability of Raindrop Size Distribution in the Mid-Atlantic Region. J. Hydrometeo., 17, 1855-1868, DOI: http://dx.doi.org/10.1175/JHM-D-15-0159.1.

Valdez, M. P., and Young K. C., 1985: Number fluxes in equilibrium raindrop populations: A Markov chain analysis. J. Atmos. Sci., 42, 1024–1036, doi:10.1175/1520-0469(1985)042<1024:NFIERP>2.0.CO;2.

Willis, P. T., and Tattelman P., 1989: Drop-size distributions associated with intense rainfall. J. Appl. Meteor., 28, 3–15, doi:10.1175/1520-0450(1989)028<0003:DSDAWI>2.0.CO;2.

Zawadzki, I., and De Agostinho Antonio M., 1988: Equilibrium raindrop size distributions in tropical rain. J. Atmos. Sci., 45, 3452–3459, doi:10.1175/1520-0469(1988)045<3452:ERSDIT>2.0.CO;2.

Captions

Figure 1. PDF (blue lines) and CDF (red lines) for convective (solid lines) and stratiform (dashed lines) samples.

Figure 2. Distribution of drop diameter corresponding to HS>0 when the identification algorithm (D'Adderio et al., 2015) is applied to 0.6-5 mm range.

Figure 3. Distribution of the samples belonging to the selected events according to their rain rate and HS. Dots indicate convective samples, while stars indicate stratiform samples.

Figure 4. Fractional occurrence of samples with EDSD (HS>0) as function of the corresponding rain rate.

Figure 5. Fractional occurrence of samples with HS>0, as function of the relative rain rate difference between each sample and the previous one.

Figure 6. Number of samples with HS>0 as function of the time difference with respect to the first observation of the event (i.e. RR>1 mm h^{-1}).

Figure 7. a) Time series of rain rate (red dot-line) and HS (blue dot-line) values, and b) DSDs of two samples of a rain event occurred on May 20, 2013 during IFloodS field campaign.

Figure 8. a) The same of Figure 6a, but for the event occurred on May 15, 2014 during IPHEX field campaign; b) DSDs preceding the equilibrium stage and EDSD.

Figure 9 a) The same of Figure 6a, but for December 29, 2013 at Wallops Island, Virginia; b) sampling of DSDs for the whole period of observation.